Available online at www.sciencedirect.com
ScienceDirect
Journal of Nuclear Materials 358 (2006) 243–254
journal of nuclear materials
www.elsevier.com/locate/jnucmat

A physical and chemical analysis of fast quenched particles of UO_2 and ZrO_2 mixture

Beong Tae Min, Jin Ho Song *, Yang Soon Park, Jong Gu Kim

Korea Atomic Energy Research Institute, 150 Dukjin dong 150, Yusonggu, Taejon 305-353, South Korea

Received 14 March 2006; accepted 28 June 2006

Abstract

An interaction between molten fuel of a nuclear reactor, which is called corium and mainly consisted of UO_2 and ZrO_2, and sub-cooled water may result in a steam explosion. It is one of the outstanding reactor safety issues. To investigate the fundamental mechanism behind the recent experimental observation that the composition of the material highly affected the strength of the steam explosion, a physical and chemical analysis for the fast quenched particles of UO_2 and ZrO_2 mixture at different compositions was performed. Six cases were selected for the study, in which the melt composition was changed, while other initial and boundary conditions of the molten fuel and water interaction tests were maintained the same. It was observed that the cases at eutectic composition resulted in a spontaneous steam explosion, while the cases at non-eutectic composition did not result in a spontaneous steam explosion. Electron probe microanalysis (EPMA) was performed for fast quenched particles along a cross-section. Results demonstrated that the UO_2 and ZrO_2 mixtures formed a solid solution of $U_{1-x}Zr_xO_2$. The mechanism for the hydrogen generation during the molten material and water interaction was examined by thermogravity analysis (TGA), X-ray diffraction (XRD) and hydrogen reduction analysis. It was demonstrated that the hydrogen generation was not directly related to the oxidation of UO_2. Morphologies observed by scanning electron microscopy (SEM) indicated that the particles from the eutectic mixture had many holes, while the particles at non-eutectic mixture did not. The existence of mush phase for the non-eutectic mixture is suggested to be the reason for the non-explosive nature.

1. Introduction

In a hypothetical severe accident of a nuclear power plant, a violent interaction between the molten core material and coolant may happen. The molten core material is called corium and mainly consisted of UO_2 and ZrO_2. Sometimes, it can lead to an energetic steam explosion. As it is one of the outstanding reactor safety issues, the risk of a steam explosion has been investigated during last decades [1]. The hydrodynamic break-up of molten liquid jet and heat transfer between the fragmented liquid drops and coolant are the major phenomena, which should be understood to quantify the potential risk of steam explosion.

* Corresponding author. Tel.: +82 42 868 2850; fax: +82 42 861 2574.
E-mail address: dosa@kaeri.re.kr (J.H. Song).

0022-3115/$ - see front matter © 2006 Elsevier B.V. All rights reserved.
doi:10.1016/j.jnucmat.2006.06.020

Recently it was observed that interaction of water with corium led to a weak steam explosion, while a non-prototypic material such as alumina resulted in an energetic explosion [2–4]. The hydrogen generation due to oxidation of UO_2 was suggested as the physical mechanism responsible for the difference [3,4], as the hydrogen gas present in the vapor film around a melt droplet could suppress the triggering of the steam explosion. As an another mechanism, an investigation on the existence of meta-stable phases during the solidification of molten reactor material and importance of surface characteristics and absorption of hydrogen gas on the strength of the steam explosion for the case of an interaction between alumina and water [5,6] was performed.

Recently, it was found that the composition of the corium highly affected the strength of the steam explosion [2]. This is an important and interesting finding from a nuclear reactor safety point of view. In this paper, a physical and chemical analysis of the fast quenched corium particles, which were produced from the interaction of molten corium at different UO_2 and ZrO_2 compositions, is reported to investigate the role of hydrogen generation and to identify the fundamental mechanism responsible for the effect of corium composition on the strength of a steam explosion.

2. Cases analyzed

The experiments were performed in the TROI test facility using corium [2]. A typical configuration of the TROI test is shown in Fig. 1. In TROI test, a liquid jet stream of molten corium at about 3000 K was discharged from the exit of the crucible into a pool of water at room temperature. Then an interaction between the molten corium and the sub-cooled water in the test section occurs. It can lead to either an energetic steam explosion or non-energetic reaction.

A cold crucible technique was used for the melting of the corium [7]. Representative shapes of cold crucible and crust after a test are shown in Fig. 2(a)–(d). UO_2 pellets and zirconia powder at given weight percent are mixed together as the initial charge material for the cold crucible. Fig. 2(a) shows the top view of the crucible after the test, which indicates that the top part of the crucible still remained after discharge of molten material through the exit of the crucible. The top crust is detached from the molten corium pool due to volumetric contraction. The lower part of the upper crust seen from the bottom exit of the crucible is shown in Fig. 2(b). The top surface of the upper crust is mainly pure zirconia, while the lower part is made of a mixture of zirconia and partially melted UO_2 pellets. The side crust and bottom crust is shown in Fig. 2(c) and (d).

A steam explosion is a rapid energy conversion process. When the coolant comes into contact with the molten fuel at the beginning, the fuel fragments and mixes with the coolant and the coolant vaporizes. The vapor film on the surface of the fuel serves as a resistance. This meta-stable state may be destroyed by the local vapor film collapse due to some instabilities. The collapsed vapor leads to direct contact between the fuel and coolant, rapidly increasing the heat transfer and vaporization. The quick pressure rise during the vaporization causes more fuel to be fragmented. The process can propagate spatially though the fuel–coolant mixture and lead to an energetic steam explosion or it can be damped and lead to a non-energetic interaction.

The quenched particles in the test section were collected after the test. Six cases were selected for the study, where the composition of the molten fuel is changed, while other initial and boundary conditions of the tests were maintained as the same. The charged composition, occurrence of steam explosion, hydrogen generation, and percentages of the debris at sizes below 0.425 mm are indicated in Table 1. The phase diagram for UO_2 and ZrO_2 binary mixture, which is drawn with data calculated from MATPRO [8], is shown in Fig. 3.

TROI-13 and TROI-36 used a mixture of UO_2 and ZrO_2 at 70:30 weight percent in composition, which is close to the eutectic composition as shown in Fig. 3. Other cases used a non-eutectic mixture. The amount of hydrogen generation in the pressure vessel was measured by gas sampling method. The amount of hydrogen was analyzed by the precision gas mass spectrometer (Finnigan MAT 271).

Table 1 indicates that the percentage of fine particles, whose size is smaller than 0.425 mm, is less than 10% for the case of TROI-17, 23, 29 and 32, which was non-explosive, while the percentage was between 19% and 40% for the cases of TROI-13 and 36, in which a steam explosion occurred. The occurrence of steam explosion was identified by the presence of a dynamic pressure wave in the test.

Typical particle size distribution is shown in Figs. 4 and 5 for TROI-23 and TROI-36, respectively. TROI-23 experiment did not result in an energetic steam explosion, while TROI-36 did. It is shown that mean particle size of TROI-36, where steam

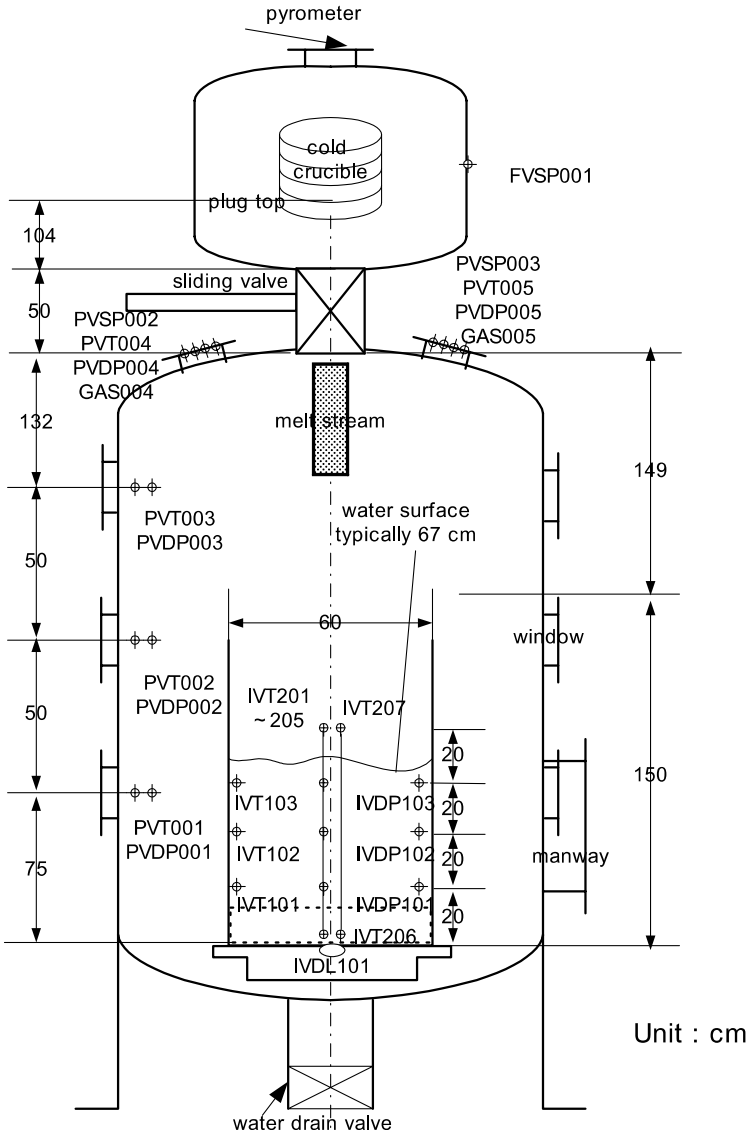

Fig. 1. A typical configuration of the TROI test.

explosion occurred, is much smaller than that of TROI-23.

Figs. 6 and 7 indicate the pressure response of the containment chamber for TROI-23 and TROI-36, respectively. The time zero indicates the time of melt stream delivery, after which it took about 1 s for the melt stream to reach free surface of the water in the test section. The pressure of the containment chamber increases because steam is generated from the test section due to a violent interaction between the fragmented melt and water. The abrupt increase in the pressure during 1–2 s for TROI-36 indicates that there was a violent steam generation. A violent steam generation was due to an abrupt increase in heat transfer from the fragmented particles. TROI-23 case without steam explosion, where the mean particle size was bigger than that of TROI-36 as shown in Figs. 4 and 5, resulted in a rather slower pressurization. It is due to a bigger mean particle size, which resulted in a less heat transfer in a given time interval.

3. Physical and chemical analyses of quenched particles

A scanning electron microscope (SEM) was used to examine the morphology of debris. The wet analysis using inductively coupled plasma-atomic

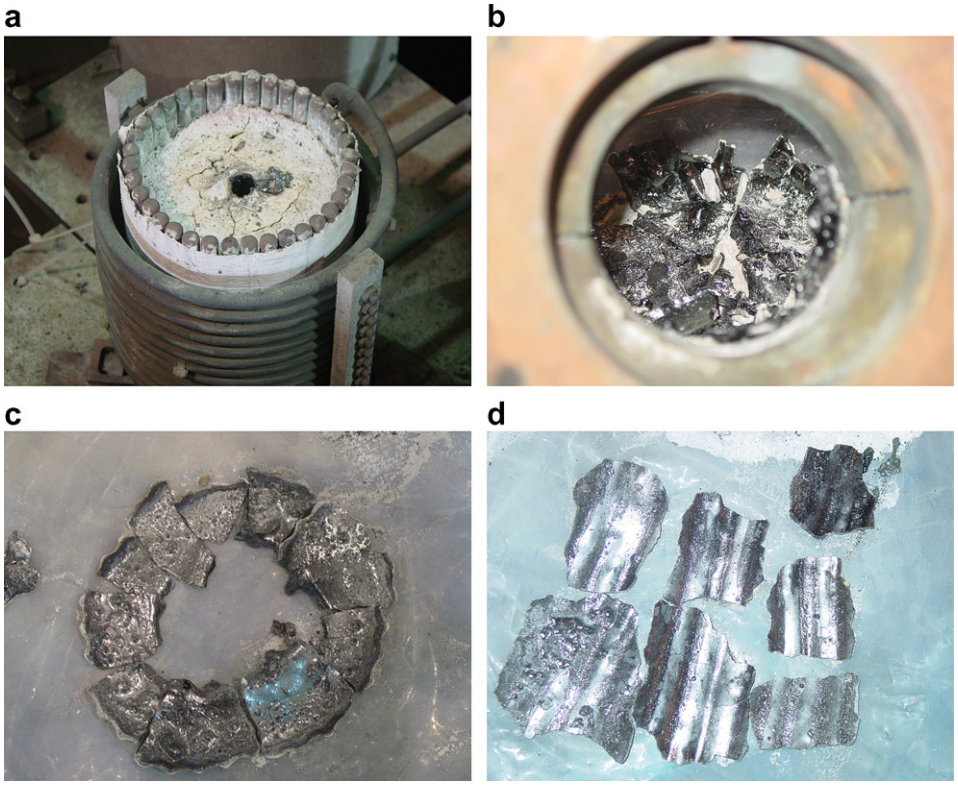

Fig. 2. Pictures of cold crucible and crusts after the experiment. (a) Top view of the crucible. (b) Top crust seen from the bottom. (c) Bottom crust. (d) Side crust.

Table 1
A summary of the test cases

Test number	Initial charge composition UO_2/ZrO_2	Steam explosion	H_2 generation (ppm)	Percentage of debris <0.425 mm
TROI-13	70/30	Yes	165	18.9
TROI-17	78/22	No	789	1.53
TROI-23	78/22	No	438	2.74
TROI-29	50/50	No	619	8.69
TROI-32	87/13	No	1010	5.32
TROI-36	70/30	Yes	14200	40.8

emission spectrometry (ICP-AES) and an elementary analysis using an electron probe microanalyzer (EPMA) were performed to identify the chemical composition of the debris. X-ray diffraction (XRD) patterns were measured for a phase characterization.

3.1. Morphologies of the quenched particles

The particles collected by a sieving screen with an opening size of 0.425 mm were subject to the analysis. By taking a sample group from the particles, the morphologies were examined by SEM. Typical morphologies of the particles for TROI-23, 29, 32, and 36 are shown in Fig. 8(a)–(d).

As TROI-17 and TROI-23, which were 80:20 composition, showed similar morphologies, typical shape for TROI-23 is shown in Fig. 8(a). It is shown that the shape is rather regular and most of the particles are at sizes near 0.425 mm, which was the sieve size. The surface had some regular patterns. Fig. 8(b) shows the morphology particles for TROI-29, which was at 50:50 composition. The average particle size was near 0.425 mm. The shape is rather regular. However, the regular pattern did not appear on the surface. Instead, some material precipitated on the surface. Fig. 8(c) shows the morphology TROI-32, which was at 90:10 composition. The average particle size was near 0.425 mm. The shape is rather regular. Similar to TROI-29 it did not have a specific pattern on the surface. These cases were non-explosive cases.

Fig. 8(d) shows a typical shape of particles for the explosive case of TROI-36. It is shown that the majority of the particles were at sizes below

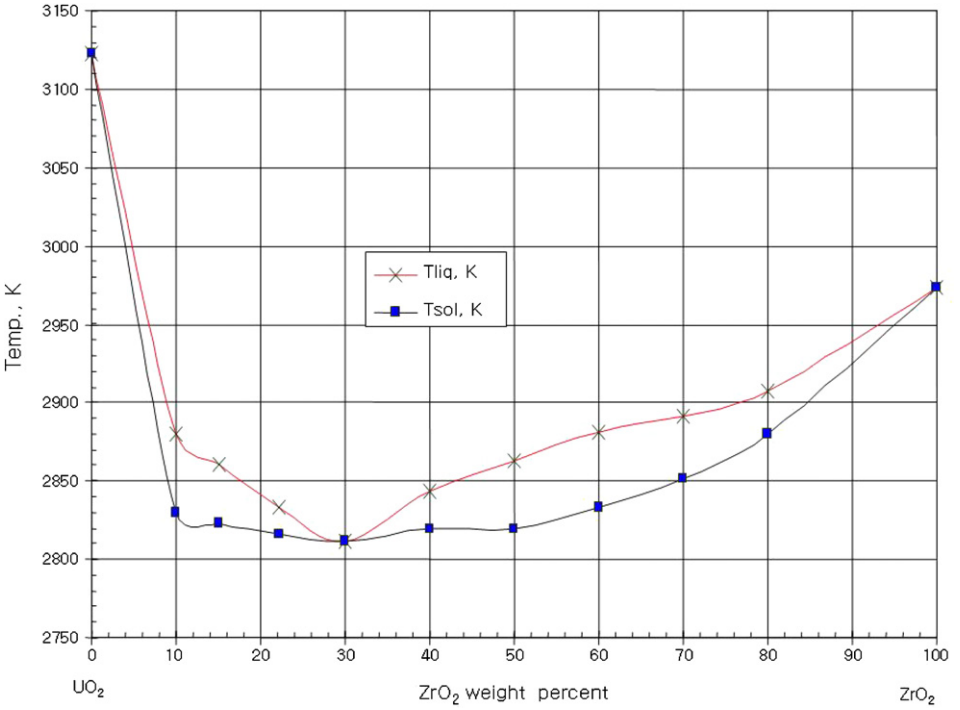

Fig. 3. Phase diagram for UO_2 and ZrO_2 binary mixture.

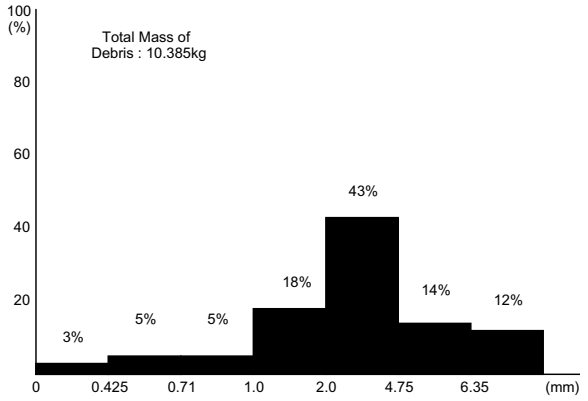

Fig. 4. Debris size distribution (TROI-23).

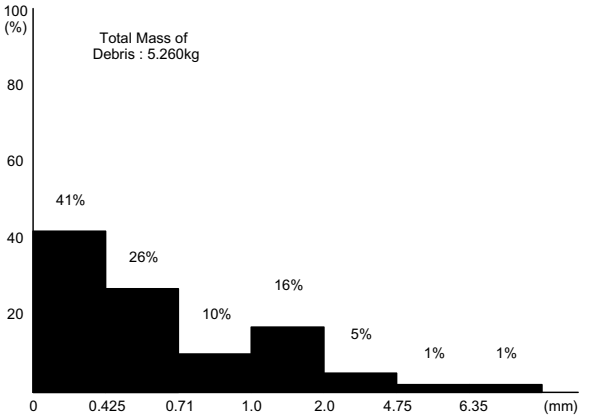

Fig. 5. Debris size distribution (TROI-36).

100 μm. The shape of the particles was rather irregular and the surface was rough. The trend was quite similar in case of TROI-13.

3.2. An analysis of the chemical composition of the particles

As the chemical composition of the particles could be different from that of the charging material, the chemical composition of the quenched particles, which would represent the composition of the molten liquid pool formed in the crucible, was analyzed.

The results of ICP-AES analysis in Table 2 indicate that the charged composition was close to that of the fast quenched melt in the water. The difference mainly came from the formation of upper crust, where pure zirconia powder was used to provide an insulation layer for the radiation heat loss. It is noted that in some cases, the results of ICP-AES did not make 100% in total due to measurement uncertainty.

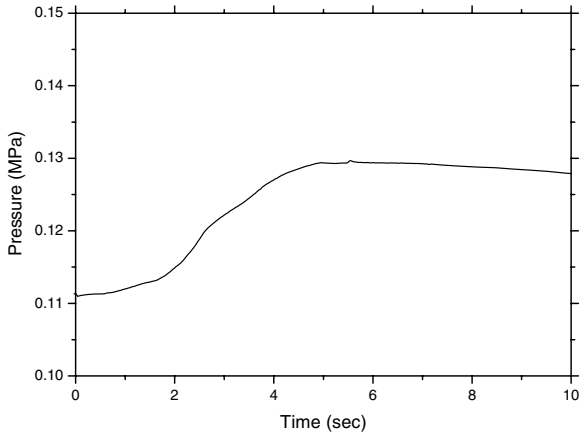

Fig. 6. Pressure of the containment (TROI-23).

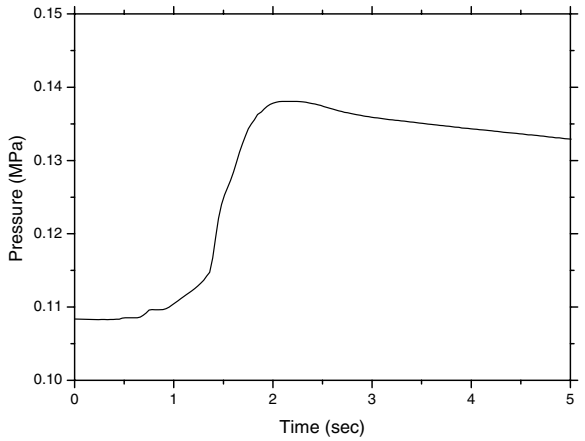

Fig. 7. Pressure of the containment (TROI-36).

Table 2 indicates that the results of wet analysis are in good agreement with those of EPMA, which were applied either on the surface of the particle or on the surface of the ground particle. EPMA for the non-eutectic debris consistently showed a higher Zr fraction than that of the wet analysis except for TROI-29. It is probable that the Zr-rich liquid might have been pushed outwards during a solidification process. TROI-29 shows a reverse behavior, since it is located on the other branch of the phase diagram. U-rich liquid might have been pushed outwards during a solidification process in this case.

3.3. Solidification behavior

To observe the internal structure of the particles, the particles were put on the resin and ground. The cross-sectional views of the particles were taken by a SEM for TROI-23, TROI-13 and TROI-36. The particles at similar size were selected for comparison, since they should have experienced similar quenching behavior. SEM photographs and results of EPMA are shown in Figs. 9–14 for each test.

The particles were either in spherical or ellipsoidal shape. Three particles were selected for each experiment to check repeatability of the data. And the UO_2 and ZrO_2 contents were examined along the radial direction at five locations for each particle.

Fig. 9(a) and (b) shows the cross-sectional views of the particles for TROI-23. Three particles indicated by a, b, and c were chosen and the magnified view of the cross-section of chosen particle is shown. It does have cracks, which was made during the solidification process due to a volume shrinkage. The composition along the cross-section for each particle for TROI-23 is shown in Fig. 10. It is shown that the composition is quite uniform along the cross-section, which indicates that UO_2 and ZrO_2 formed a solid solution of $U_{1-x}Zr_xO_2$ [5]. The abrupt change in the composition for particle 'c' indicates that the Zr rich liquid was pushed outwards during solidification. It is noted that as the particle 'b' has a large aspect ratio, the composition was scanned along a longer direction.

In case of TROI-13, the composition was close to eutectic composition. Fig. 11(a) and (b) indicates that there are many holes in the particles. The composition by EPMA was uniform as shown in Fig. 12 and the average value was not much different with the charged percentage or ICP-AES analysis.

In case of TROI-36, the trend was similar to that of TROI-13 as can be seen from Figs. 13 and 14. There are more holes at bigger size than TROI-13. The composition by EPMA was quite uniform along the cross-section of the particle and the average was not much different with the charged percentage or ICP-AES analysis and it is interesting that holes are not present in the particles of TROI-23, while the particles of TROI-13 and 36, whose composition is close to eutectic composition, have many holes. The reason for this behavior can be explained as below.

A binary mixture exists as mush phase, when the melt temperature is between the solidus and liquidus temperature [9]. As the corium is a mixture of oxide, it has low thermal conductivity. So the core part of the particle remained as either a liquid phase or a much phase, while the surface layer of the particle is being solidified.

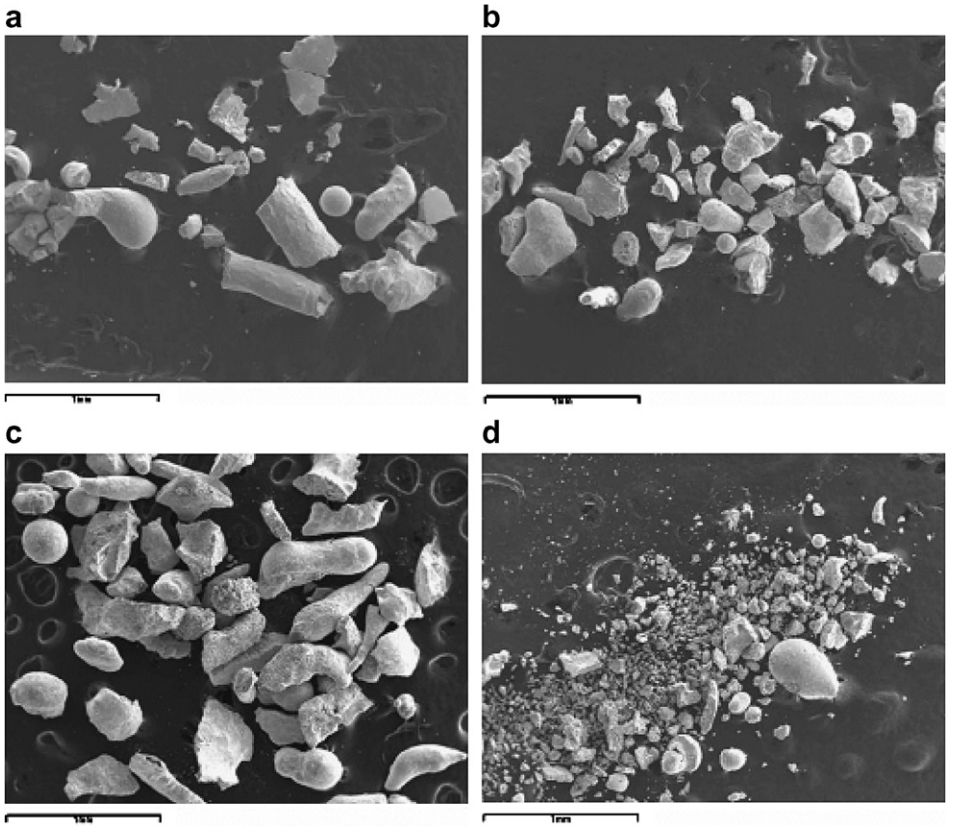

Fig. 8. Morphology of particles. (a) Particles for TROI-23. (b) Particles for TROI-29. (c) Particles for TROI TROI-32. (d) Particles for TROI TROI-36.

Table 2
Results of chemical analysis

Test	Initial charge composition UO_2/ZrO_2	ICP-AES composition	EPMA composition
TROI-13	70/30	70.09/27.22	72.05/27.95[a]
TROI-17	78/22	*69.2/19.1*	69.17/30.83
TROI-23	78/22	78.62/20.40	75.79/24.21[a]
TROI-29	50.0/50.0	*52.2/45.1*	61.01/38.99
TROI-32	87/13	85.65/12.02	83.87/16.13
TROI-36	70/30	74.54/25.46	70.73/29.27[a]

[a] These samples were ground. Other samples are EPMA on the surface.

The solidification behavior of eutectic material and non-eutectic material would be different. For the non-eutectic mixture, the solid nuclei in the mush phase would become nucleation sites. So it could result in a uniform solidification, if the population of nuclei is high. It argument is supported by the cross-sectional view of the particles for TROI-23, the structure of the cross-section is uniform and only cracks due to density difference are observed. For the eutectic material, the core part of the particle remains as liquid, while the surface layer solidifies. It would have much less number of nucleation sites. So, the tension between the liquid in the core and the solidified surface layer had resulted in a formation of many holes in the particle, which is demonstrated in the cross-sectional views of the particles for TROI-13 and 36.

It is highly probable that eutectic corium particles with many pores inside would be more fragile to the pressure wave than the non-eutectic corium with less pores during the propagation of explosion. It would certainly affect the fine fragmentation behavior during the propagation of explosion, because substantial amount of particles would be at this temperature range during the molten corium and water interaction process before it is solidified.

Therefore, it is suggested that a different solidification behavior between the eutectic material and non-eutectic material discussed above could be the

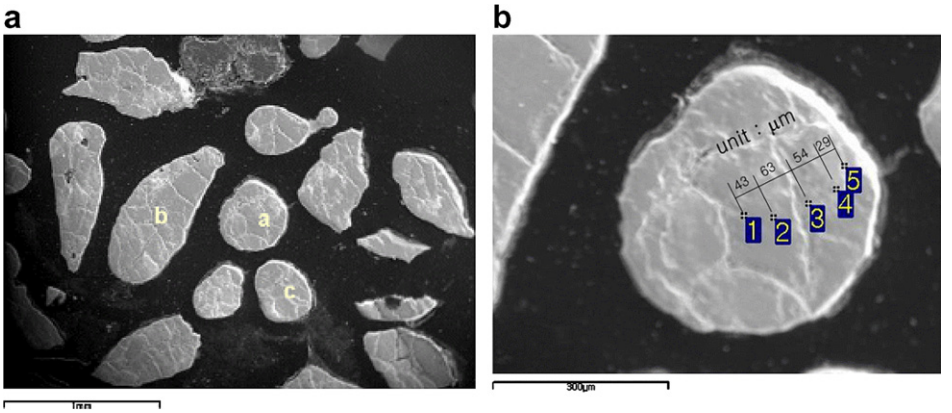

Fig. 9. Particles of TROI-23 subject to SEM and EMPA. (a) Debris, magnification 40. (b) Debris 'a', diameter 440 μm.

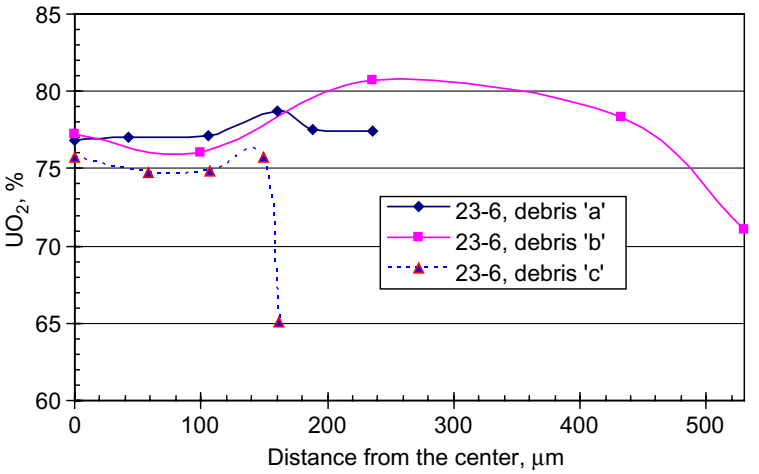

Fig. 10. The composition along the cross-section for each particle for TROI-23.

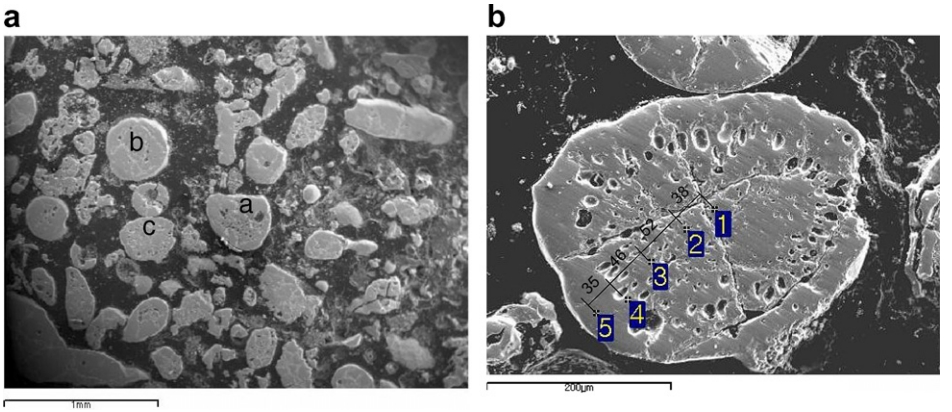

Fig. 11. Particles for TROI-13 subject to SEM and EPMA. (a) Debris, magnification 40. (b) Debris 'c', $W \times D = 420 \times 385$ μm.

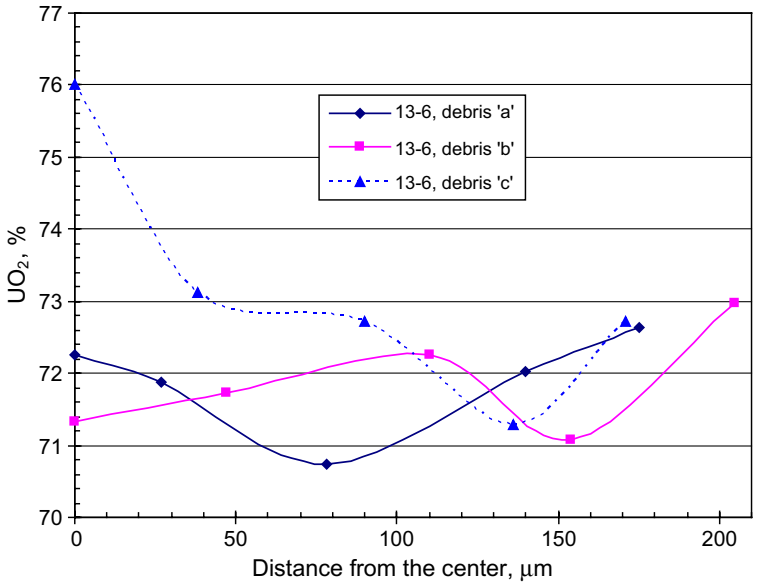

Fig. 12. The composition along the cross-section for each particle for TROI-13.

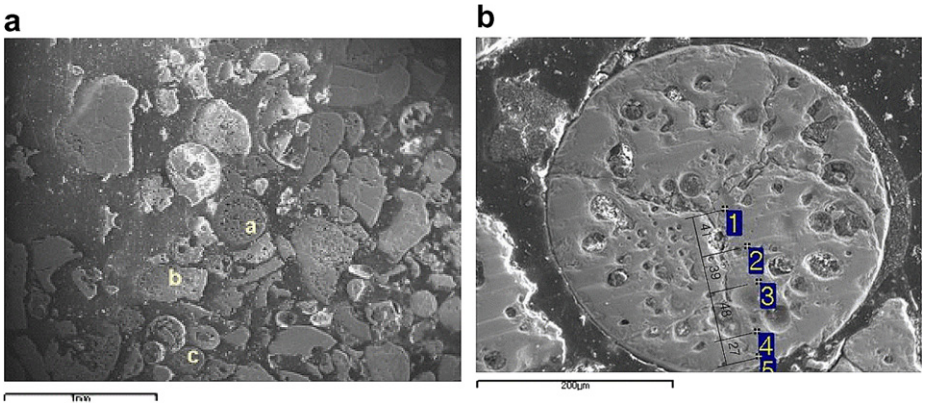

Fig. 13. Particles for TROI-36 subject to SEM and EPMA. (a) Debris, magnification 40. (b) Debris 'a', diameter 340 μm.

fundamental mechanism for the difference in the strength of steam explosion.

3.4. Hydrogen generation

In FARO experiments [3], a large amount of hydrogen gas was observed and it was suggested that the oxidation of UO_2 to U_3O_8 during melting and/or quenching in the water could explain the hydrogen generation [3]. Therefore, evidence for the oxidation of UO_2 was investigated by thermogravity analysis (TGA), hydrogen reduction, and X-ray diffraction (XRD) for the particles from the TROI experiment.

In the thermogravity analysis the sample specimen was oxidized *by heating at a rate of* 10 °C/min between 20 and 1000 °C. The measured increase in the weight percent by a TGA analysis for the specimen was 1.68% as shown in Fig. 15. From the equation below, it is estimated that a full oxidation from UO_2 to U_3O_8 would result in a weight increase of 3.95% in case of pure UO_2. So, it is possible that 77.06% of UO_2 was oxidized during TGA process and 22.94% of the debris could be U_3O_8 or there is another mechanism which inhibits oxidation of UO_2.

$$3UO_2 + 2H_2O \rightarrow U_3O_8 + 2H_2 \quad (1)$$

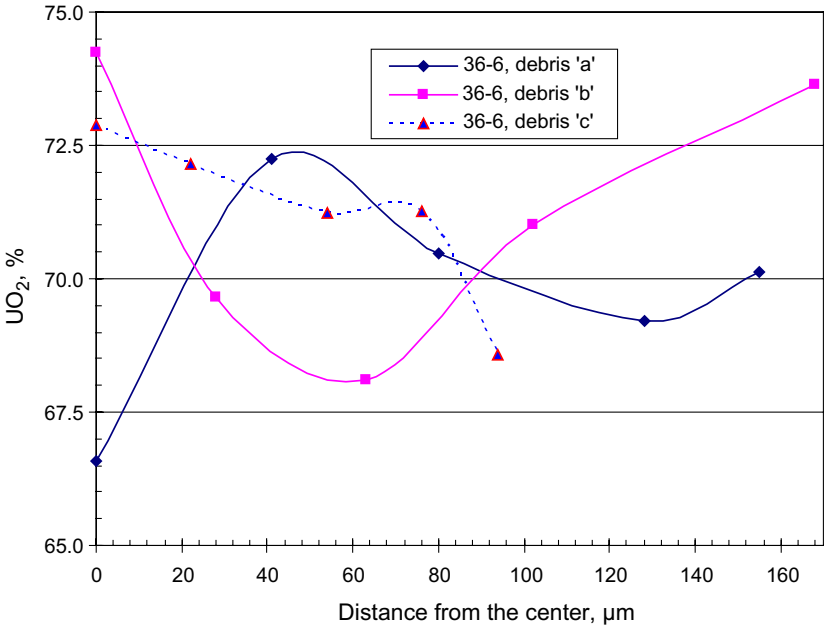

Fig. 14. The composition along the cross-section for each particle for TROI-36.

To investigate the source of hydrogen generation, a XRD analysis was performed for TROI-36. The results of XRD analysis in Fig. 16 indicate that peaks for either U_3O_8 or ZrO_2 did not appear. It is highly probable that ZrO_2 peak did not appear because ZrO_2 and UO_2 formed solid solution in the form of $U_{1-x}Zr_xO_2$ species, which was suggested in Piluso et al. [6]. So, it is probable that there was an inhibition effect due to a formation of $U_{1-x}Zr_xO_2$ solid solution in the TGA analysis.

To confirm this conclusion, the debris of TROI-36 were reduced under a hydrogen atmosphere at temperature 1700 °C for 12 h, but their weight did not change. It confirmed that there was no U_3O_8 in the

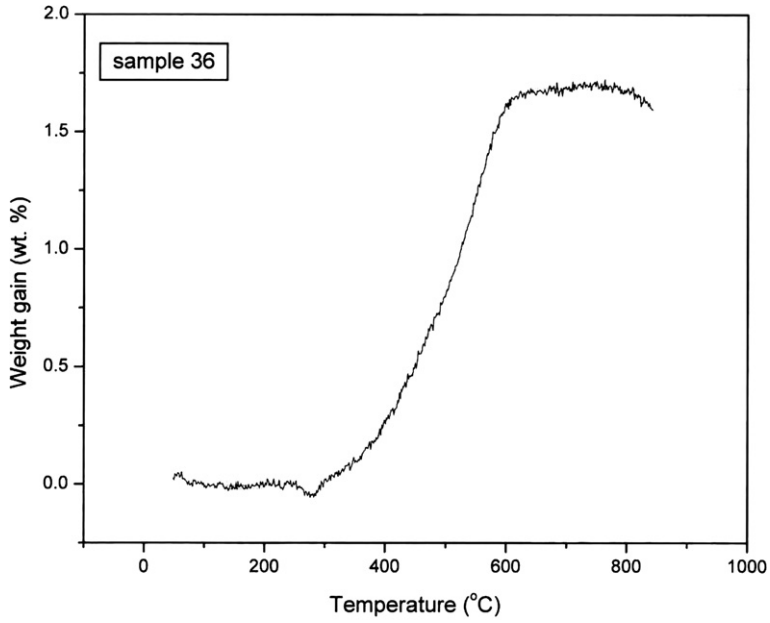

Fig. 15. TGA result for TROI-36 debris.

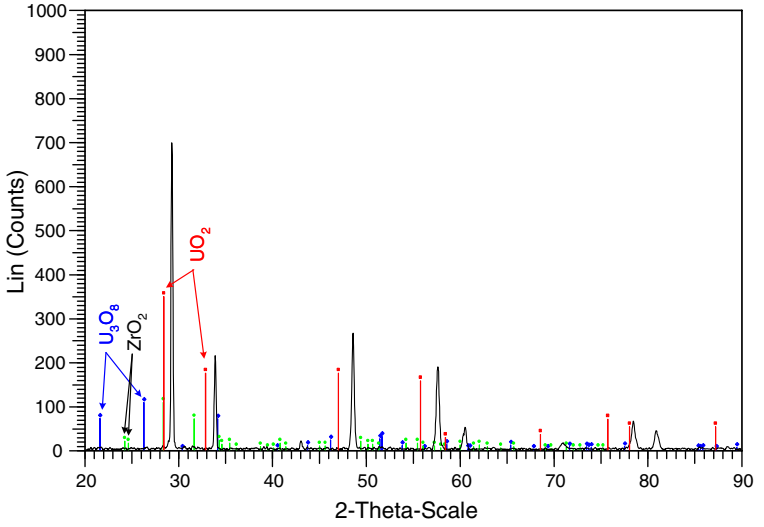

Fig. 16. XRD results for TROI-36 particle.

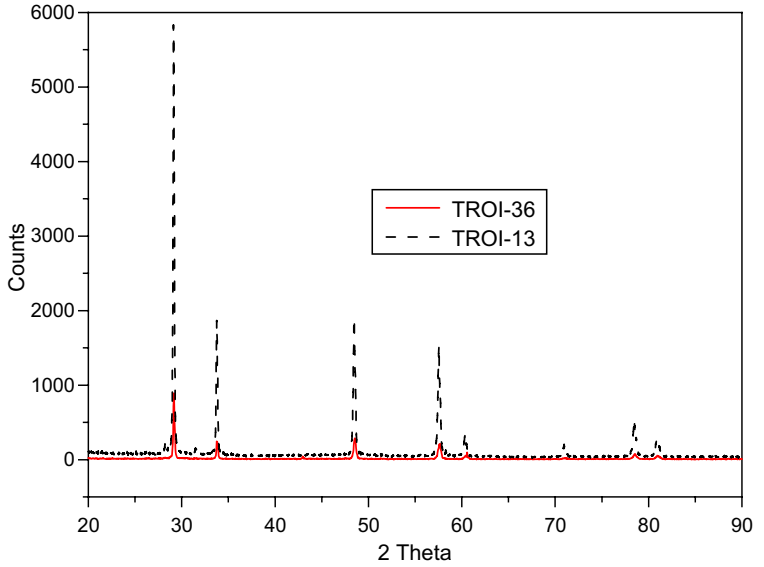

Fig. 17. Comparison of XRD patterns for TROI-13 and TROI-36.

debris. It is concluded that the reason for the generation of hydrogen is not relevant to the oxidation of UO_2, which was suggested as the potential reason. It is consistent with the experimental results that substantial amount of hydrogen generation was seldom observed in the TROI experiments. It could be due to a dissociation of water at a very high temperature.

A XRD analysis was performed for the particles of TROI-13. It was found that the XRD pattern was almost the same as that of TROI-36 as shown in Fig. 17. It is noted that the counts for TROI-13 was much larger, as it was exposed during a much longer time than TROI-36. It confirms the argument that the hydrogen generation is not directly related to both the oxidation of UO_2 and occurrence of steam explosion.

4. Conclusions

A physical and chemical analysis of the fast quenched particles, which experienced a molten fuel and coolant interaction, was performed. The results of eight cases at different composition of UO_2 and ZrO_2 mixture indicate that the case with steam explosion was near eutectic composition, while the

case without steam explosion was at non-eutectic composition.

The electron probe microanalysis (EPMA) for a fast quenched particle along a cross-section indicated that UO_2 and ZrO_2 mixture formed a uniform solid solution. The source of hydrogen generation was investigated by thermogravity analysis (TGA), XRD and hydrogen reduction analysis. It is shown that the hydrogen gas generation was not directly related to either the oxidation of UO_2 or steam explosion.

It is suggested that there is a material effect due to the existence of a mush phase, which affects the fine fragmentation behavior, in turn, triggering and maintaining a steam explosion. Comparative cross-sectional views of the corium particles by scanning electron microscope supported the proposed argument.

Acknowledgements

This study has been carried out under the nuclear R&D program by the Korean Ministry of Science and Technology.

References

[1] B.R. Sehgal, Accomplishments and Challenges of the Severe Accident Research, NURETH-9, San Francisco, 3–8 October 1999.
[2] J.H. Song et al., Nucl. Eng. Des. 222 (2003) 1.
[3] D. Magallon, I. Huhtiniemi, H. Hohmann, Nucl. Eng. Des. 189 (1999) 223.
[4] D. Magallon, I. Huhtiniemi, Nucl. Eng. Des. 204 (2001) 369.
[5] P. Piluso, G. Trillon, C. Journeau, J. Nucl. Mater. 344 (2005) 259.
[6] P. Piluso, G. Trillon, D. Magallon, in: Proceedings of ICAPP'05, Seoul, Korea, 15–19 May 2005, Paper 5268.
[7] S.W. Hong, B.T. Min, J.H. Song, H.D. Kim, Mater. Sci. Eng. A357 (2003) 297.
[8] L.J. Siefken, E.W. Coryell, E.A. Harvego, J.K. Hohorst, SCDAP/RELAP5/MOD2 Code Manual, vol. 4; MATPRO – A library of Materials Properties for Light Water Reactor Accident Analysis, NUREG/CR-5273, EGG-2555, vol. 4, 1990.
[9] T.N. Dinh, A.T. Dinh, J.A. Green, B.R. Sehgal, An assessment of steam explosion potential in molten-fuel coolant interaction experiments, in: 6th International Conference on Nuclear Engineering, ICONE-6365, ASME, 1998.